Energy 71 (2014) 367–376

Contents lists available at ScienceDirect

Energy

journal homepage: www.elsevier.com/locate/energy

Multi-objective and multi-parameter optimization of a thermoelectric generator module

Jing-Hui Meng [a], Xin-Xin Zhang [a], Xiao-Dong Wang [b,c,*]

[a] School of Mechanical Engineering, University of Science and Technology Beijing, Beijing 100083, China
[b] State Key Laboratory of Alternate Electrical Power System with Renewable Energy Sources, North China Electric Power University, Beijing 102206, China
[c] Beijing Key Laboratory of Multiphase Flow and Heat Transfer for Low Grade Energy, North China Electric Power University, Beijing 102206, China

ARTICLE INFO

Article history:
Received 24 January 2014
Received in revised form
19 April 2014
Accepted 22 April 2014
Available online 17 May 2014

Keywords:
Thermoelectric generator
Output power
Conversion efficiency
Multi-objective and multi-parameter optimization

ABSTRACT

A multi-objective and multi-parameter optimization is implemented to design the optimal structure of bismuth-telluride-based TEG (thermoelectric generator) module. A multi-physics TEG model combining the SCG (simplified conjugate-gradient) algorithm is used as the optimization tool. The semiconductor pair number, leg length, and base area ratio of semiconductor columns to TEG module significantly affect the TEG performance, and hence are all incorporated into the present optimization study. A single-objective optimization is first implemented to provide input parameters for the multi-objective optimization. The results show that when taking the output power as the single-objective function, the output power can be elevated significantly by optimization of the three geometric parameters but which also accompanies the significant reduction in the conversion efficiency. The same result also occurs when taking the conversion efficiency as the single-objective function. By combining the output power and conversion efficiency with a weight factor as the multi-objective function, the optimization is again implemented. The optimal design obtained by multi-objective optimization makes a proper balance between the output power and conversion efficiency, so that the both are improved simultaneously.

1. Introduction

TEGs (thermoelectric generators) are based on the Seebeck effect of semiconductor materials to convert thermal energy to electricity directly [1,2]. In recent years, thermoelectric technology is attracting more and more attention, mainly because of the following two aspects: on the one hand, there are not working fluids or other moving parts, so TEs (thermoelectric devices) have many good features, such as reliable operation, layout flexibility, adaptability and other characteristics [3,4]; on the other hand, TEs do not produce secondary pollution gases such as carbon dioxide or other unfriend polluting gases in the progress of using the life or industrial waste heat for electricity generation [5,6].

Previous studies show that the TEG performance, including the output power (P) and conversion efficiency (η), is strongly dependent on semiconductor material properties. In general, the dimensionless figure of merit is adopted to represent the influence of material properties on the TE (thermoelectric device) performance, which is defined as $ZT = \alpha^2\sigma T/\lambda$, where α is the Seebeck coefficient, σ is the electric conductivity, λ is the thermal conductivity, and T is the absolute temperature at which the properties are measured [7]. A larger ZT represents better performance of TEs, therefore, researchers who are engaged in thermoelectric materials are committed to enhancing ZT, which means increasing the Seebeck coefficient and electric conductivity, and at the same time keeping thermal conductivity values as low as possible [8,9]. Minnich et al.'s research [8] showed that bulk nanostructured thermoelectric materials have the most promise for commercial use due to their plasticity and compatibility. Tang and Zhang [9] found that the ZT of thermoelectric material $Fe_xCo_{4-x}Sb_{12}$ ($x = 0$–3) can be improved significantly by filling Ce, Ba, and Y.

Except for thermoelectric materials, the impact of the geometry on the TEs performance cannot also be ignored. TEs geometry optimization can be divided into two categories: one is the single-parameter optimization [10–15], and the other is multi-parameter optimization using various inverse problem approaches [16–19]. Up to now, the single-parameter optimization is the most widely used method. For example, Jang et al. [10] adopted the single-parameter method to study how the thickness of ceramic plate,

* Corresponding author. State Key Laboratory of Alternate Electrical Power System with Renewable Energy Sources, North China Electric Power University, Beijing 102206, China. Tel./fax: +86 10 62321277.
E-mail address: wangxd99@gmail.com (X.-D. Wang).

http://dx.doi.org/10.1016/j.energy.2014.04.082
0360-5442/

Nomenclature

P	output power (W)
η	conversion efficiency
COP	coefficient of performance
ZT	figure of merit
T	temperature (K)
f	weight factor
C	search variable
A_{total}	area of TEG module base
J	objective function
N	semiconductor pair number
A_{pair}	base area of TEG unit
A_{pn}	cross-sectional area of p- or n-type semiconductor
H	height (mm)
W	width (mm)

Abbreviation

TEG	thermoelectric generator
TEC	thermoelectric cooler

Greek letters

α	Seebeck coefficient (V K^{-1})
σ	electric conductivity (S m^{-1})
λ	thermal conductivity (W m^{-1} K^{-1})
ρ	electric resistivity (Ω m^{-1})
Δ	difference
β	search step size
π	search direction
γ	base area ratio of semiconductor columns to TEG module

Subscripts

opt	optimal
pn	p- or n-type semiconductor
Cu	copper
k	number of variables

Superscript

n	number of iterations

foot length and cross-sectional area of the p- or n-type semiconductor affect the performance of a micro TEG (thermoelectric generator) unit. They found that for each of the three geometry parameters, there is always a specific size corresponding to the optimal P or η, however, the optimal P and η cannot be reached simultaneously. Yu et al. [11] lay emphasis on the influences of the junction temperature difference (ΔT_2) in the second stage, the length of thermocouples (L_1) and the NUM (number of thermocouples) in the first stage on the cooling performance of a two-stage TEC module. They included that: 1) For a fixed ΔT_2, the decreases of L_1 and NUM can improve the coefficient of performance ; 2) When keeping a constant coefficient of performance, the decreases of L_1 and NUM can also decrease ΔT_2, and thus increase the cooling capacity. Chen et al. [12] proposed a new cycle model consisting of a multi-couple thermoelectric device and involving several key irreversibilities of real TEGs to optimize the value of $(S_p/l_p)n$, where S_p and l_p are the cross-sectional area and leg length of p-type semiconductor, n is the number of couples. For the fixed total number of thermoelectric elements of two-stage thermoelectric refrigerator driven by two-stage thermoelectric generator, Meng et al. [13] optimized the allocations of the thermoelectric element pairs for the maximum cooling load and coefficient of performance. Yilbas and Sahin [14] examined the influence of the slenderness ratio and the external load parameter on the maximum efficiency of a TEG, and found that the efficiency attains high values for the slenderness ratio less than 1 for almost all the external load parameters considered, which is more pronounced for the large values of the external load parameter. Optimizations were carried out for the two-stage TE coolers with two design configurations, i.e., the pyramid-styled and cuboid-styled ones by Xuan et al. [15], the optimum number ratio of TE modules between two stages for the first design and the optimum electric current ratio between two stages for the second design were finally obtained.

In all the single-parameter optimization studies [10–15], the optimal value for a specific parameter is obtained by searching this parameter to reach the optimal TE performance while keeping the other parameters unchanged. However, because all the parameters have coupled effects on the TE performance, the optimal TE performance cannot be reached only by searching a specific parameter. Fortunately, a few studies [16–19] have made attempt to develop TEC (thermoelectric cooler) multi-parameter optimization methods by combining the various optimization algorithms and the TEC analytical/numerical model. Cheng et al. combined a TEC model and a genetic algorithm to optimize of the geometry of single- [16] and double-stage [17] TEC. In their study, the maximum cooling capacity was defined as the objective function under the requirement of minimum coefficient of performance and the constraint of maximum material cost. The leg length, the leg area and the number of legs were taken as search variables and were optimized simultaneously. Rao and Patel [18] developed a modified version of the teaching–learning-based optimization algorithm and incorporated this algorithm into the TEC model to optimize the performance of double-stage TEC. The cold stage current, hot stage current, and number ratio of thermoelectric elements between the two stages were three search variables. Thermal resistance model was adopted as the direct problem solver in Refs. [16–18]. Due to grossly simplifying assumptions, such as that only the energy balance equations at the hot and cold ends were solved, only constant or temperature-averaged properties can be used, the current density vector was simplified as a constant scalar, etc., the thermal resistance model, however, cannot predict the TE performance accurately, and therefore is not appropriate as the direct problem solver for TE optimization. Recently, we combined a multi-physics TEC model [19] and a SCG algorithm to optimize the cooling capacity of a TEC module. A value of COP (coefficient of performance) that was not lower than 70% COP of the initial TEC geometry was chosen as the constraint condition, and the semiconductor pair number, the leg length, and the base area ratio of semiconductor columns to TEC were taken as search variables. The optimal geometry corresponding to the maximum cooling capacity was successfully obtained, however, the COP of the optimal geometry was reduced as compared with the initial geometry.

The motivation of the present work is based mainly on the following three points: 1) the effect of the TEG geometry on its performance is also very significant, however, the TEG multi-parameter optimization has not been reported so far; 2) as two important evaluation indexes for the TEG performance, P and η cannot reach the extreme value simultaneously when using the single-objective optimization, hence, multi-objective optimization needs to be carried out; 3) it is well known that the direct problem solver is very critical for the optimization, due to the limitation of

the thermal resistance model, the optimization needs to adopt the multi-physics TEG model as the direct problem solver. In the present work, the TEG multi-objective optimization approach is first developed, which is composed of a SCG algorithm and a multi-physics TEG model. The approach is then used to optimize a micro-TEG module. By taking the weighted average of P and η as the multi-objective function, three search variables, semiconductor pair number, leg length, and base area ratio of semiconductor columns to TEG module, are optimized simultaneously to look for the optimal TEG performance.

2. Numerical methods

2.1. Optimization approach

Typically, an inverse problem optimization approach includes a direct problem solver and an inverse problem solver. To ensure the successful optimization, the multi-physics TEG model [20–22] developed previously by our group is adopted as the direct problem solver. The multi-physics TEG model solves the temperature and electric potential equations, and accounts for all effects occurred in TEG, including Seebeck effect, Peltier effect, Thomson effect, Joule heating, Fourier heat conduction, and temperature-dependent properties. The TEG model was proven to be complete self-consistency [20], which also has been well validated by comparing the prediction with the experimental data and the analytical solution [21,22], and its accuracy is greatly improved as compared with the thermal resistance model [23]. More details of the model can be found in Refs. [20–22].

There are many optimization algorithms, such as the genetic algorithm, conjugate-gradient algorithm, Newton–Raphson algorithm, adaptive weighting input estimation algorithm, and simulated annealing algorithm. The genetic algorithm and simulated annealing algorithm search in the direction of a better design, but randomly mutate from this direction in case there might be a better solution elsewhere. The advantage of this type of algorithms is that they are able to find the global solution among multiple local minima. The disadvantage is that they require a very large number of design evaluations and cannot present how the optimized parameters approach their optimal values. Another class of algorithms is known as gradient algorithms. These algorithms use information about how a change in each design variable affects the objective function. The gradient algorithms such as conjugated-gradient algorithms calculate the partial derivative of the objective function with respect to each design variable and use the information to select design variable values for an improved design. The advantage of gradient algorithms is that once the gradients are calculated they are efficient. Therefore, the present work adopted the conjugated-gradient algorithm as the optimization algorithm. Determining the optimal search step size for conventional conjugated-gradient procedures is complex and time-consuming. Cheng and Chang [24] developed a simplified version of the conjugated-gradient algorithm that uses a constant step size in each iteration and applies a direct numerical differentiation method to determine search direction. The simplified conjugated-gradient algorithm has been applied successfully to optimize the geometric structures of proton exchange membrane fuel cells [25], micro-channel heat sinks [26], and TEC [19] in our previous studies. Therefore, this algorithm is chosen as the inverse problem solver.

2.2. TEG module geometry and optimized parameters

Fig. 1a is the schematic of a TEG module, which comprises two bases with the area of $A_{total} = 4 \times 4$ mm^2, N pairs of TEG units connected electrically in series and thermally in parallel. Each TEG unit (Fig. 1b) has the base area of $A_{pair} = A_{total}/N$ and consists of three metal connectors, a p-type semiconductor and a n-type semiconductor. The p- and n-type semiconductors have the same dimension with the height of H_{pn} and the cross-sectional area of $A_{pn} = W_{cu} \times W_{cu}$. The height of the copper connector is H_{Cu} and the width is W_{cu}. The metal connector is made of copper, the p- and n-type semiconductors are bismuth-telluride materials. Table 1 lists all the material properties. It is noted that the Seebeck coefficient, electrical conductivity and thermal conductivity of semiconductors are all temperature-dependent.

For the TEG module with a fixed A_{total}, once the semiconductor pair number (N), the leg length (H_{pn}), and the base area ratio of semiconductor columns to TEG module ($\gamma = 2NA_{pn}/A_{total} = 2A_{pn}/A_{pair}$) are specified, the TEG module geometry will be determined uniquely. The effect of single parameter N, H_{pn} or γ on the TEG module performance is shown in Fig. 2. Here the cold end temperature is assumed to be 300 K with the temperature difference of $\Delta T = 150$ K. $N = 40$, $H_{pn} = 0.5$ mm and $\gamma = 0.80$ are defined as the base-line geometry. In the single-parameter analysis, only one parameter of interest is changed while the other two parameters keep the values of the base-line geometry. Fig. 2 shows that N, H_{pn} and γ all significantly affect the TEG module performance. Consequently, the three parameters are chosen as the search variables.

Fig. 2 also shows that for the output power the optimal parameter is $N = 60$, $H_{pn} = 0.06$ mm, and γ approaching to 1, however, it becomes $N = 55$, $H_{pn} = 0.68$ mm, and $\gamma = 0.60$ for the conversion efficiency. It can be expected that when the output

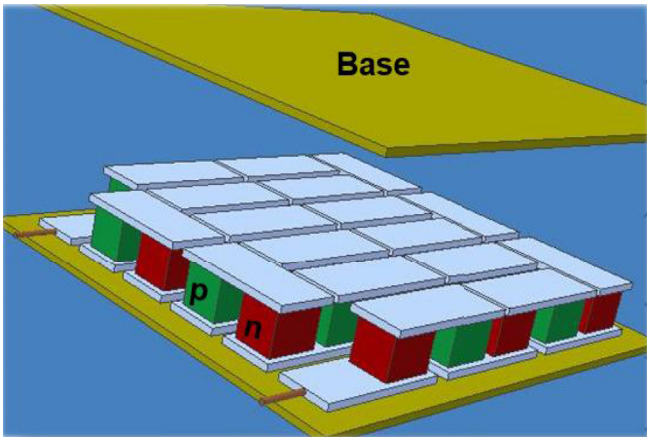

(a)

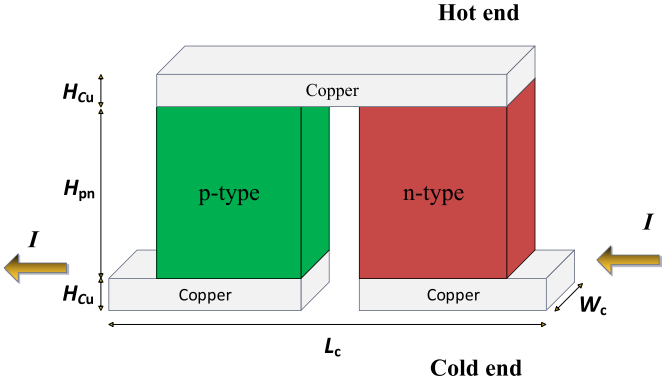

(b)

Fig. 1. Schematics of a TEG module and a TEG unit: (a) TEG module; (b) TEG unit.

Table 1
Material properties used in this paper.

Parameters	Semiconductor (bismuth-telluride)	Connector (Cu)
λ (W K^{-1} m^{-1})	$k_p = k_n$ $0.000029T^2 - 0.019593T + 4.809677$	350
ρ (Ω m)	$\rho_p = \rho_n$ $10^{-6}(0.043542T - 2.754139)$	1.695×10^{-9}
α (V K^{-1})	$\alpha_p = -\alpha_n$ $10^{-6}(-0.002025T^2 + 1.423448T - 44.953611)$	–
Source	[27]	[10]

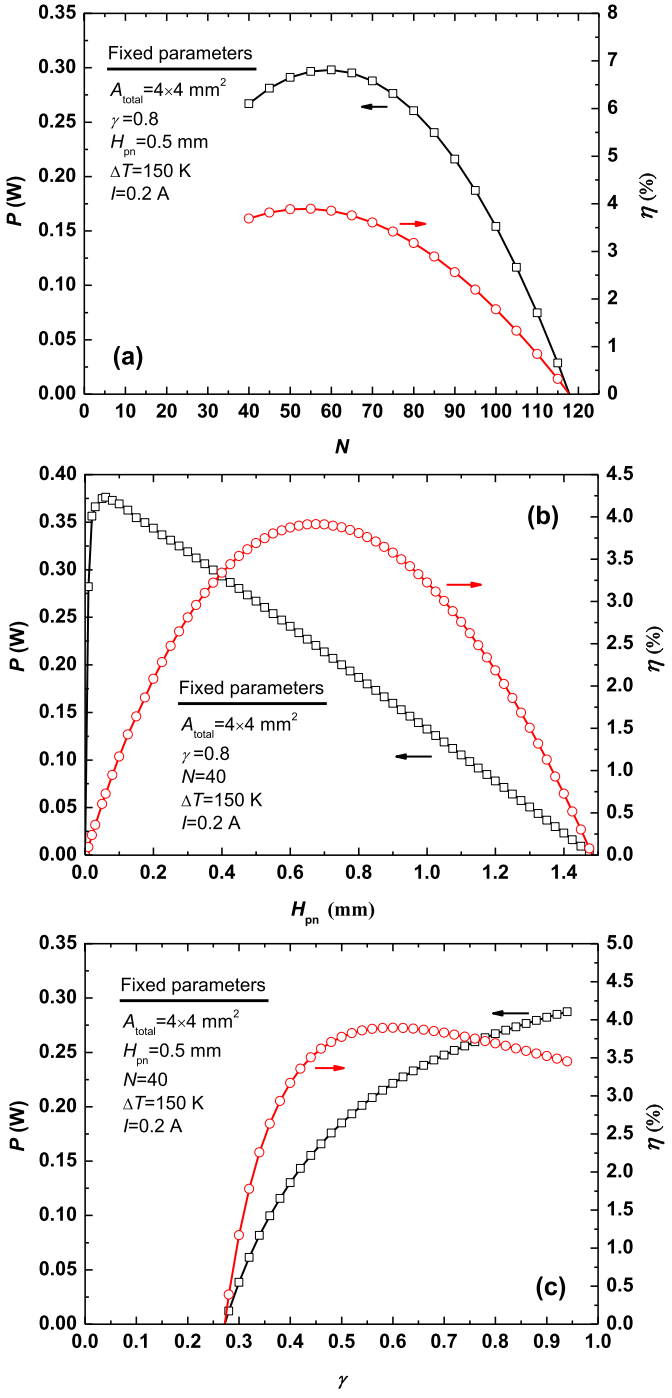

Fig. 2. The effect of single parameter on TEG performance: (a) N; (b) H_{pn}; (c) γ.

power servers as the objective function, the maximum output power can be reached by looking for optimal parameter combination of N, H_{pn}, and γ, while the conversion efficiency may be reduced significantly. Similarly, the maximum conversion efficiency is reached at the cost of the output power. Therefore, two objectives namely maximizing the output power and maximizing the conversion efficiency of the TEG module are considered simultaneously for multi-objective optimization. In present optimization, the multi-objective function is defined as follows:

$$J = f\frac{P}{P\text{opt}} + (1-f)\frac{\eta}{\eta_{\text{opt}}} \tag{1}$$

where, f is a weight factor for the first objective function P, P_{opt} is the maximum value of the objective functions P and η_{opt} is the maximum value of the objective function η, when these objectives are considered independently.

2.3. Constraint condition

Before the optimization, it is necessary to give the reasonable range of search variables based on the practical requirements. Although single parameter analysis revealed that a small H_{pn} and a large γ can improve P of the TEG module, due to the limitation of the actual processing, H_{pn} cannot be arbitrarily small, and γ cannot be equal to 1. In addition, larger N means smaller TEG unit, which will bring processing difficulties, therefore, the constraint condition of the optimization are chosen as $N \leq 200$, $H_{pn} \geq 0.1$ mm, and $\gamma \leq 0.95$.

2.4. Optimization procedure

Fig. 3 shows the flow chart of optimization procedure. For convenience, the search variables C_1, C_2 and C_3 are used to denote the semiconductor pair number N, the leg length H_{pn}. The procedure for applying the simplified conjugated-gradient algorithm is described briefly as follows. Step 1: Make an initial guess for the search variables $C_1 \sim C_3$ and the values of the search step sizes $\beta_1 \sim \beta_3$, with initialization accomplished, the run itself can begin. Step 2: Use the direct problem solver to predict the TEG module performance, and calculate the objective function J. Step 3: When the objective function reaches a maximum, the solution process is terminated, otherwise, proceed to step 4. Step 4: Determine the gradient functions, $\partial J/\partial C_k$ ($k = 1, 2, 3$). Step 5: Calculate the conjugate-gradient coefficients, γ_k^n, and the search directions, $\pi_k^{(n)}$, for each of the search variables. Step 6: Assign a fixed value to the step sizes β_k ($k = 1, 2, 3$) for all the search variables, and leave it unchanged during the iteration. Step7: Update the search variables and go back to step 2.

3. Validation of the optimization approach

It is well known that, similar with other gradient algorithms, the simplified conjugated-gradient method may not find the global minimum of the objective function, it can get trapped in local minimum solutions. The solution that the simplified conjugated-gradient method arrives at depends on the configuration of the initial design. Thus, several restarts may be required to find the global solution. Based on the reason above, three sets of initial values of search variables, ($N = 40$, $H_{pn} = 0.5$, $\gamma = 0.80$), (60, 0.4 mm, 0.70) and (80, 0.6 mm, 0.60), are used in our optimization. Taking P as the single-objective function, the multi-parameter optimization is carried out and the results are shown in Fig. 4. The output powers are 0.16 W, 0.23 W and 0.18 W for the three initial designs, then they gradually increase as the TEG geometry is optimized, and

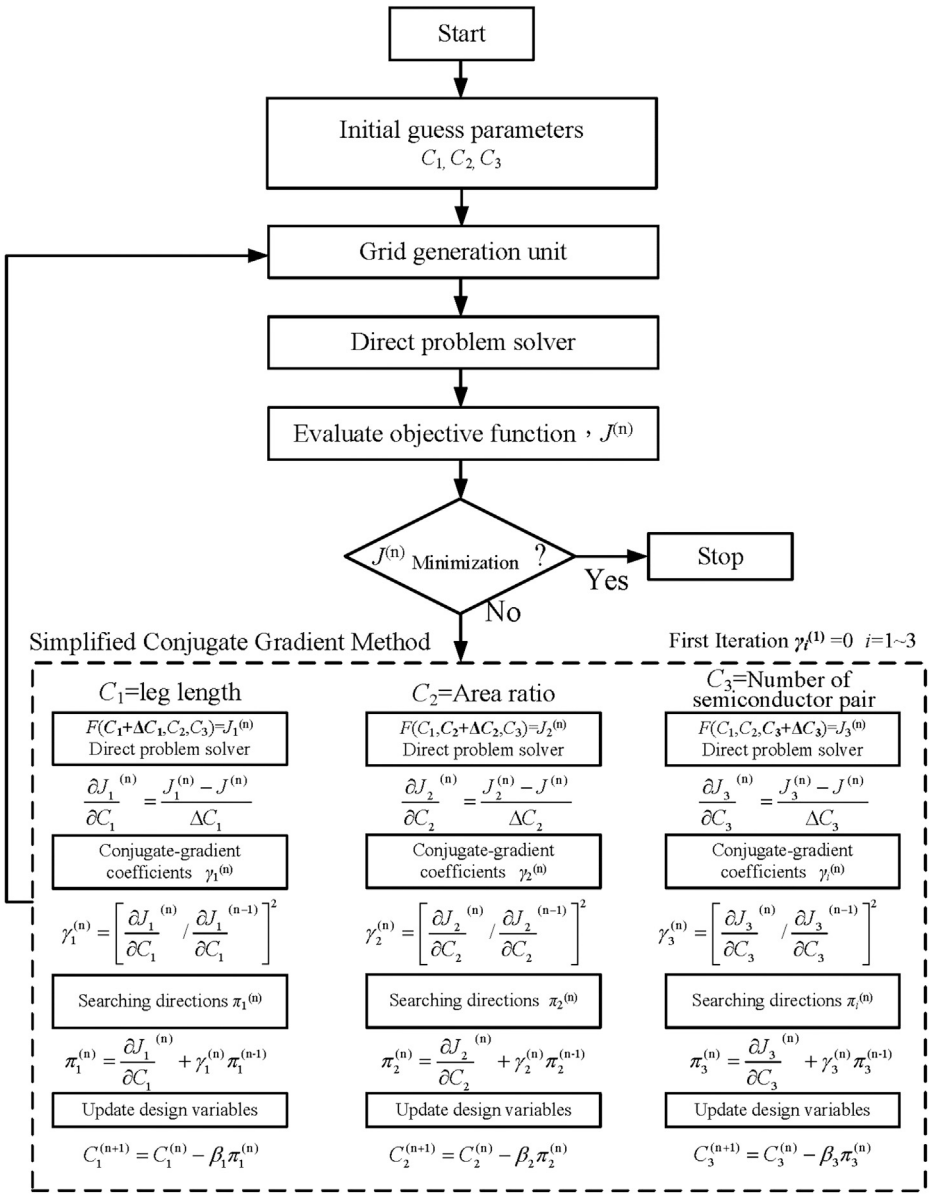

Fig. 3. Flow chart of optimization procedure.

finally reach the same maximum value of $P_{max} = 0.53$ W at search step 96, 70, and 64. The results show that the initial values of each search variable for the three initial designs differ significantly, however, the same optimal design is reached, which indicates that the obtained optimal design may be a global maximum solution for the objective function. Compared with the initial designs, the output power rises by 231.25%, 130.43%, and 194.44%, respectively. Fig. 4b shows that the conversion efficiency for the optimal design is 0.72%, which is much lower than that of the three initial designs (2.46%, 3.00% and 3.67%). This again confirms our analysis above, when using a single objective function, it is difficult to simultaneously maximize the output power and the conversion efficiency.

4. Results and discussion

A micro-TEG module with the base area of only 4 × 4 mm^2 is selected as the testing example to display applicability of the present multi-objective and multi-parameter optimization approach for TEG geometry design. Due to the dependence of P and η on the applied current, it can be expected that the optimal geometry of the TEG module should vary at different load currents. Therefore, the search variables with initial values of $N = 40$, $H_{pn} = 0.50$ mm, $\gamma = 0.80$ are optimized simultaneously to look for the optimal geometry at $\Delta T = 150$ K with load currents of $I = 0.10$ A, 0.25 A, 0.30 A, and 0.50 A. The selected load currents represent the typical small, medium, and large currents. It should be pointed that the initial design has the maximum η at $I = 0.25$ A and the maximum P at $I = 0.30$ A.

4.1. Single-objective optimization

To determine P_{opt} and η_{opt} in the multi-objective function (Eq. (1)), two single-objective optimizations with P and η as the objective function are first implemented. Fig. 5 shows the evolutions of η and P during optimization when taking η as the objective function. For the initial design, η is 2.46%, 3.79%, 3.74%, and 1.61%

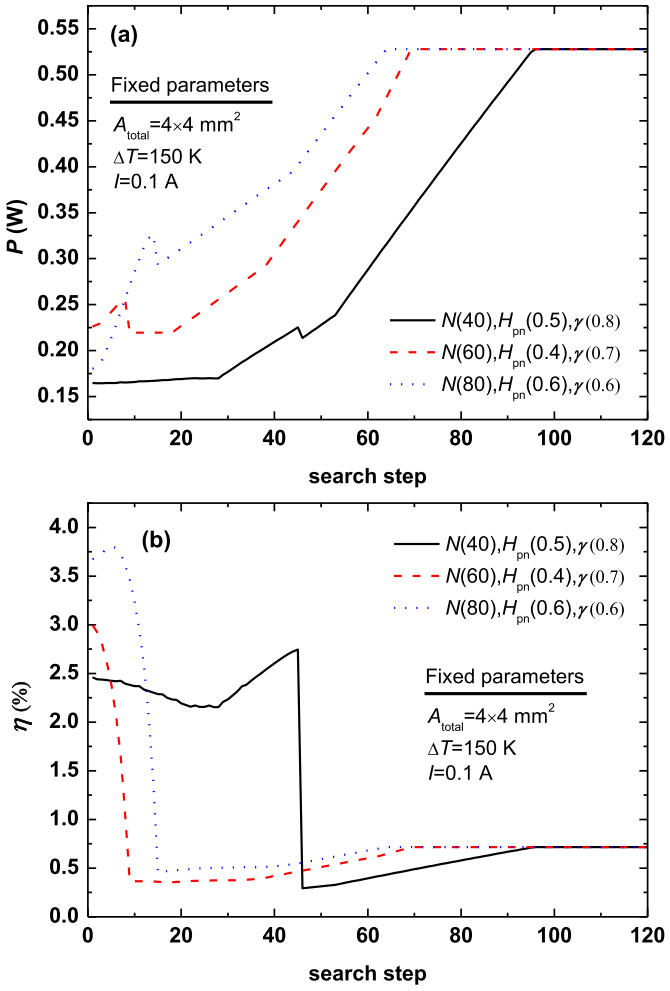

Fig. 4. Variations of TEG performance during optimization using the three initial designs: (a) P; (b) η.

at $I = 0.10$ A, 0.25 A, 0.30 A, and $I = 0.50$ A. When the TEG module reaches the optimal design, η respectively increases to 3.84%, 3.86%, 3.85%, and 3.85%. For $I = 0.10$ A and 0.50 A, η is improved significantly, about 56.10% and 139.13% higher than those of the initial design. However, for $I = 0.25$ A and 0.30 A, η increases only by 1.85% and 2.94%. This is mainly due to the following two reasons. First, when thermoelectric materials and temperature difference are specified, the difference between maximum conversion efficiencies for TEG modules with various designs is relatively small. Second, the initial design of the TEG module reaches or approaches the maximum η at these two currents, so that the space for the improvement of η is small. Fig. 5b shows that when taking η as the objective function, P of the optimal design presents two different change trends depending on the load current. At small and medium currents of $I = 0.10$ A, 0.25 A and 0.30 A, P of the optimal design is 0.13 W, 0.17 W, and 0.19 W, lower than 0.16 W, 0.28 W, and 0.30 W of the initial design. However, at the large current of $I = 0.50$ A, P of the optimal design is 0.20 W, high than 0.14 W of the initial design. This means that it is possible to simultaneously increase η and P, and hence the multi-objective optimization is necessary and achievable. Fig. 6 shows evolutions of the three search variables during optimization. The optimal design depends on the load current. The optimal design has $N = 48$, $H_{pn} = 0.74$ mm, $\gamma = 0.55$ at $I = 0.10$ A; $N = 25$, $H_{pn} = 0.83$ mm, $\gamma = 0.77$ at $I = 0.25$ A; $N = 23$, $H_{pn} = 0.73$ mm, $\gamma = 0.76$ at $I = 0.30$ A; and $N = 15$, $H_{pn} = 0.75$ mm, $\gamma = 0.84$ at $I = 0.5$ A.

Fig. 7 shows evolutions of P and η during optimization when taking P as the objective function. The output power, P, is significantly improved as the three search variables are optimized and finally reaches the maximum value (Fig. 7a), while η either increases or decreases depending on the load current (Fig. 7b). The output power of the initial design is 0.16 W, 0.28 W, 0.29 W, 0.14 W at $I = 0.10$ A, 0.25 A, 0.30 A, and 0.50 A, which is elevated to 0.59 W, 1.16 W, 1.27 W, and 1.39 W, respectively. At small and medium currents, as expected, η of the optimal design is lower than that of the initial design, however, at large current of 0.5 A, P and η are improved simultaneously. It worth noting that the improvement of P is more significant at higher currents, P of the optimal design at $I = 0.50$ A exceeds that at $I = 0.3$ A, although the initial design has maximum P at $I = 0.30$ A.

4.2. Multi-objective optimization

The single-objective optimization usually improves the output power at the cost of the conversion efficiency and vice versa, therefore, the multi-objective optimization is implemented with aim to enhance P and η simultaneously. Note that the value of weight factor f in Eq. (1) may vary between 0 and 1, and any value

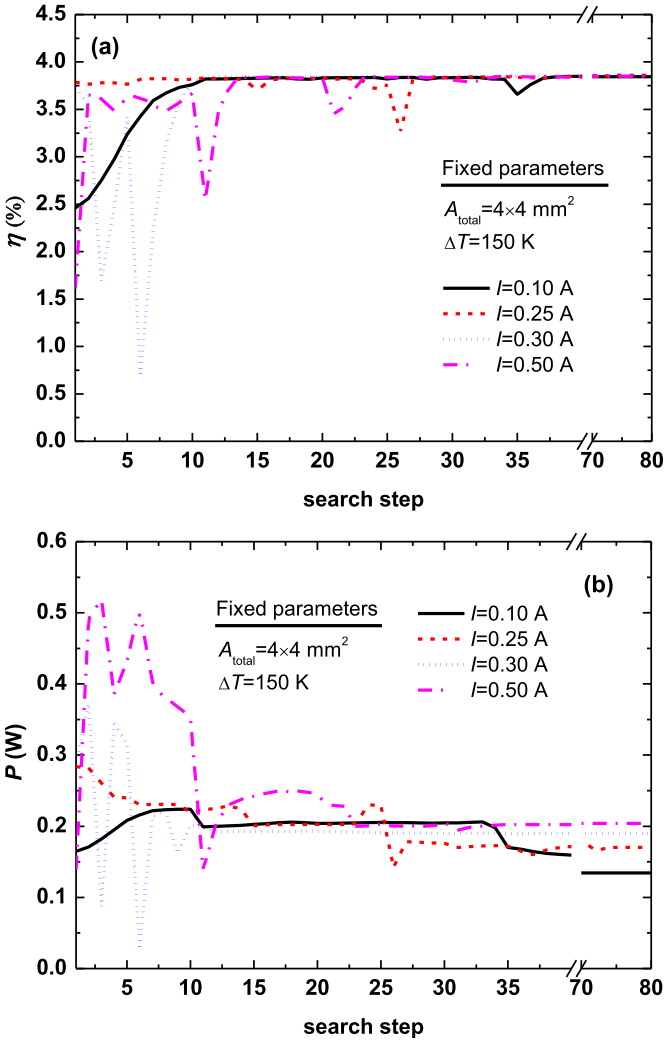

Fig. 5. Variations of TEG performance during optimization of η: (a) P; (b) η.

gives the relative importance to the single-objective function. The value of weight factor can be decided by the designer, and a value of 0.5 is adopted here.

Fig. 8 shows the evolutions of the multi-objective function, J, during optimization. The initial value of J is 0.46, 0.61, 0.60, and 0.26 at $I = 0.10$ A, 0.25 A, 0.30 A, and 0.50 A. As the geometry of the TEG module is optimized, J increases and finally reaches 0.81, 0.85, 0.89,

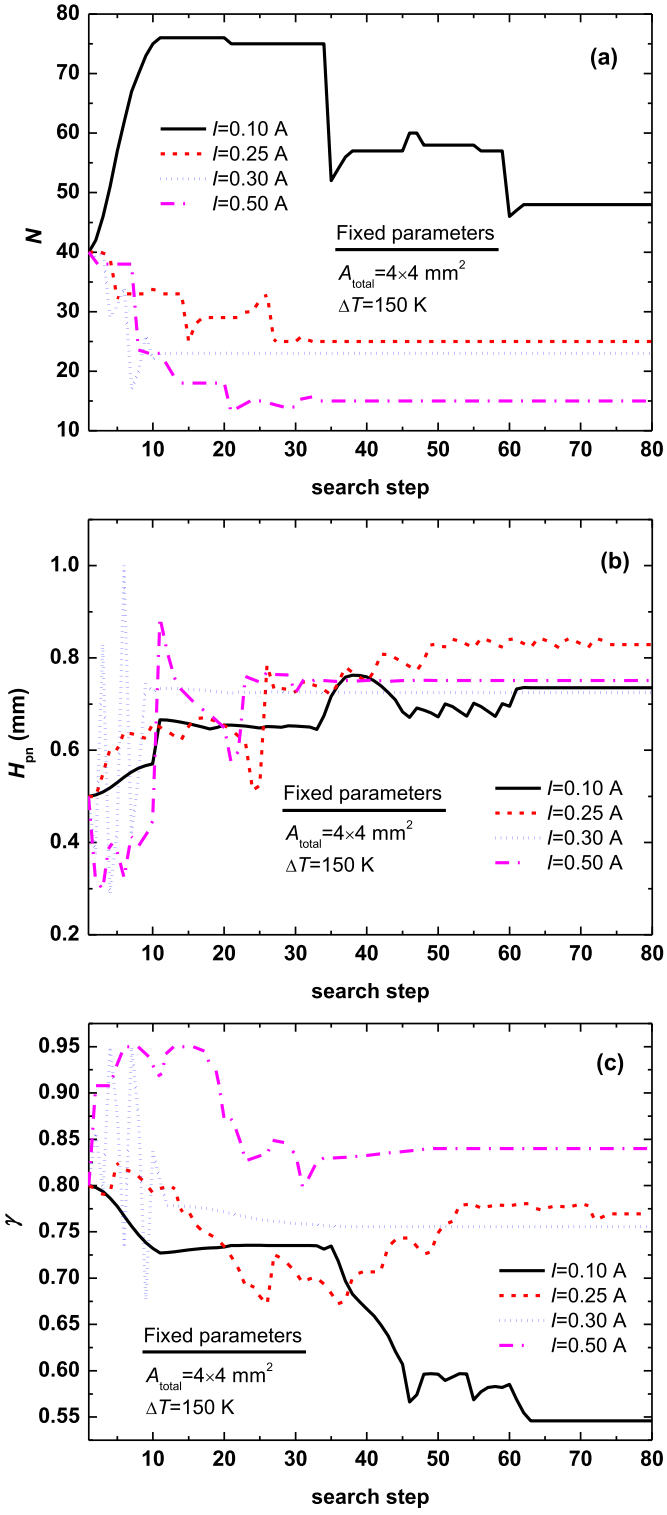

Fig. 6. Variations of search variables during optimization of η: (a) N; (b) H_{pn}; (c) γ.

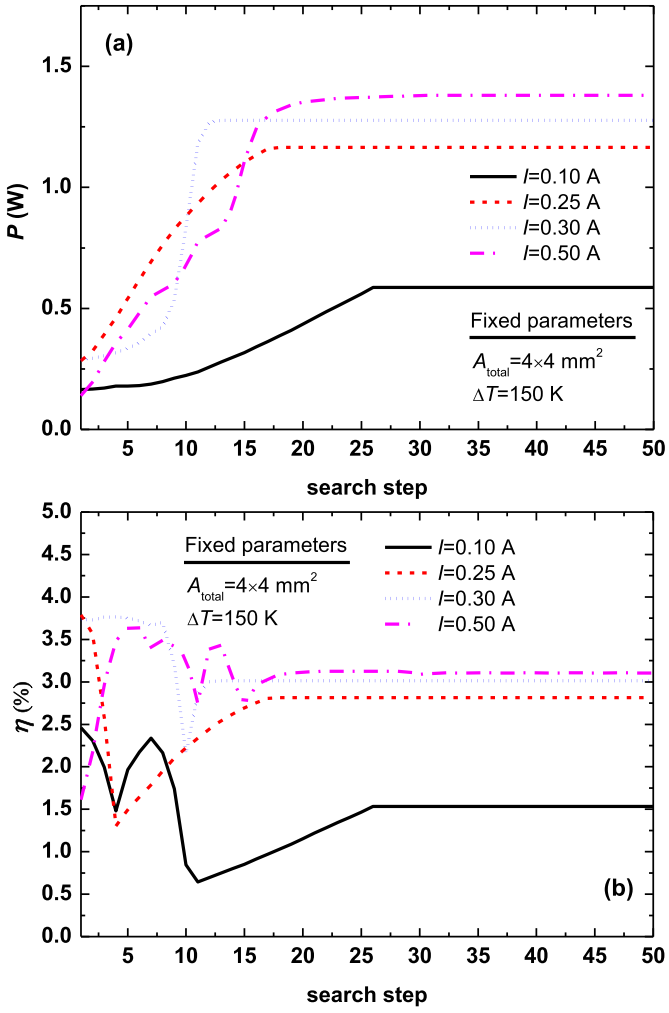

Fig. 7. Variations of TEG performance during optimization of P: (a) P; (b) η.

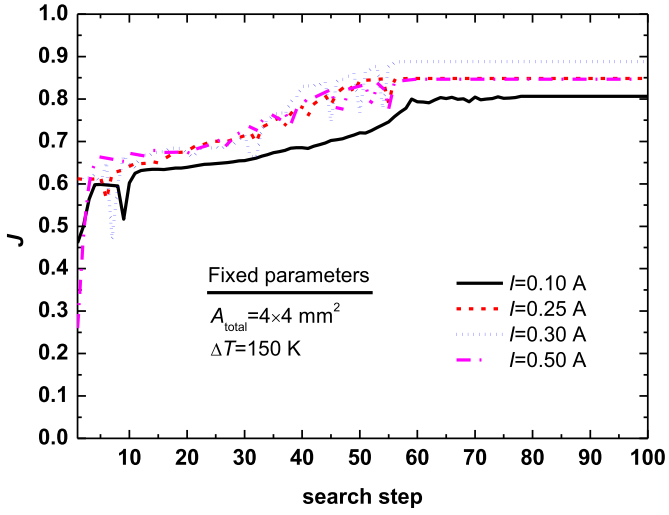

Fig. 8. Variations of the multi-objective function (J).

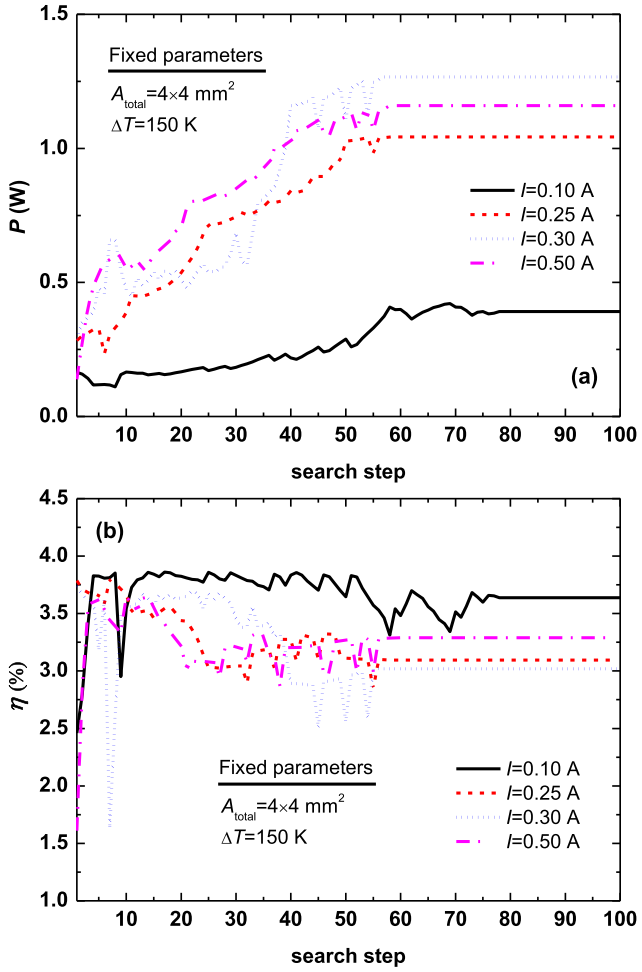

Fig. 9. Variations of TEG performance during optimization of J: (a) P; (b) η.

and 0.85, respectively. According to Eq. (1), a large J means that P and η are closer to their maximum value obtained in the single-objective optimization, however, J always cannot be equal to 1 unless the weight factor are taken as 0 or 1.

Fig. 9 shows evolutions of P and η of the TEG module during multi-objective optimization. The output power of the optimal design is found to be 0.39 W, 1.04 W, 1.27 W, and 1.16 W, and the conversion efficiency of the optimal is 3.64%, 3.10%, 3.02%, and 3.29%. In single-objective optimization, the output power of the optimal design is 0.13 W, 0.17 W, 0.19 W, and 0.20 W when taking the conversion efficiency as the objective function, while the conversion efficiency is 1.53%, 2.82%, 3.01%, and 3.10% when taking the output power as the objective function. Comparison between these data indicates that the multi-objective optimization makes a reasonable balance between P and η to improve the both simultaneously. Fig. 10 shows evolutions of the three search variables during multi-objective optimization, the optimal design has $N = 125$, $H_{pn} = 0.40$ mm, $\gamma = 0.95$ at $I = 0.10$ A; $N = 137$, $H_{pn} = 0.13$ mm, $\gamma = 0.95$ at $I = 0.25$ A; $N = 150$, $H_{pn} = 0.10$ mm, $\gamma = 0.95$ at $I = 0.30$ A; and $N = 93$, $H_{pn} = 0.13$ mm, $\gamma = 0.95$ at $I = 0.5$ A. It is noted that the optimal designs for the multi-objective optimization require a large N and a small H_{pn}, which are significantly different from those for the single-objective optimization (Fig. 6).

Fig. 11 compares the I–P and I–η curves of the initial and optimal TEG modules. The solid circles in Fig. 11 represent P or η of the optimal design, while the hollow circles are their initial values. It can be seen that the multi-objective optimization not only significantly elevates P, but also improves η. The interval of effective load current, which is defined as the current interval when $P > 0$, changes after optimization. For example, the maximum effective load current for the initial design is 0.58 A, it decreases to 0.27 A for

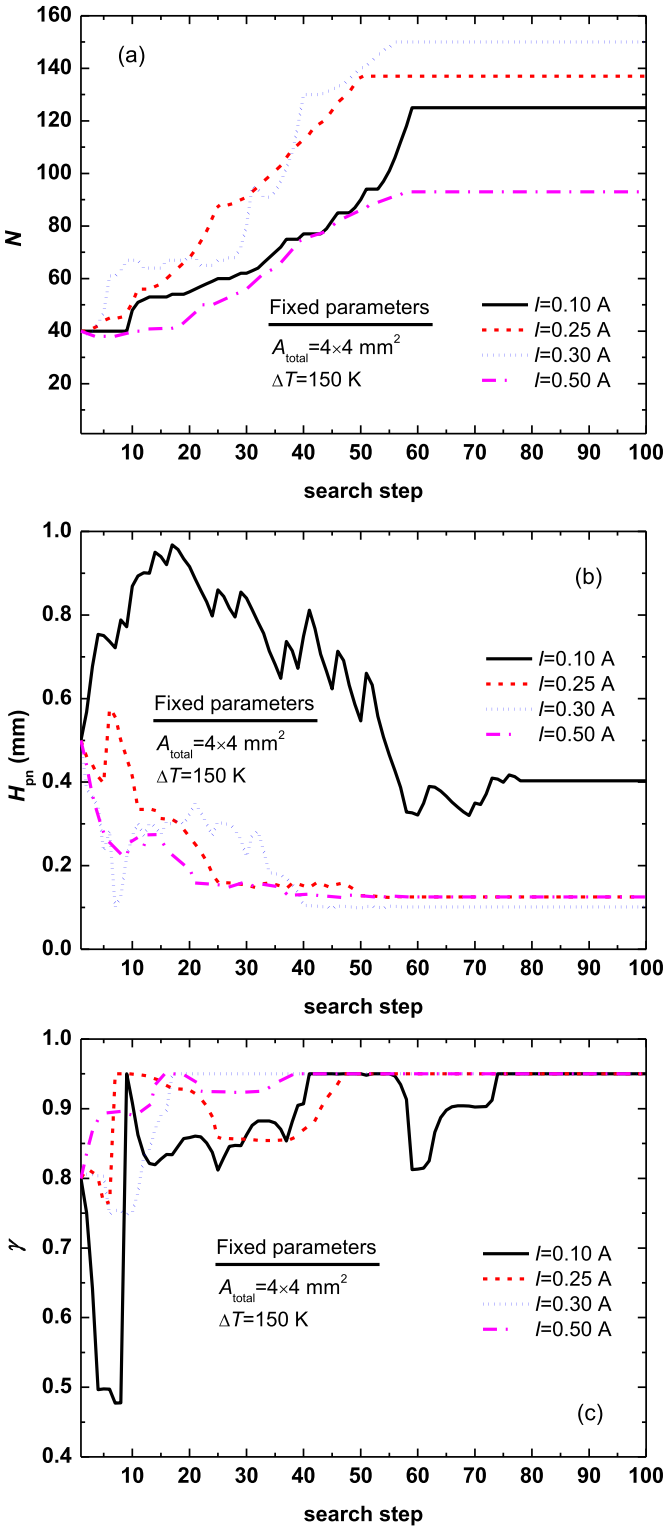

Fig. 10. Variations of search variables during multi-objective optimization: (a) N; (b) H_{pn}; (c) γ.

the optimal design obtained at $I = 0.1$ A, while increases to 1.16 A for the optimal design obtained at $I = 0.5$ A.

5. Conclusions

This paper develops an optimization approach to design the optimal structure of TEG module. In the present optimization approach, the direct problem solver adopts a multi-physics TEG numerical model which has been proved to be able provide enough accurate prediction of the TEG performance, the inverse problem solver uses a SCG algorithm. The optimization approach is tested for a bismuth-telluride-based TEG module with 4×4 mm^2 base area. The single-objective and multi-objective optimizations are respectively implemented to look for the optimal TEG performance. Three geometric parameters, semiconductor pair number N, leg length H_{pn}, and base area ratio of semiconductor columns to TEG module γ, are taken as search variables, which are optimized simultaneously.

When taking the output power P as the objective function, P is elevated significantly by optimization of the three geometric parameters. The output power of the optimal design is found to be 0.59 W, 1.16 W, 1.27 W at $I = 0.10$ A, 0.25 A, 0.30 A, and 0.50 A, about 269%, 314%, 338%, and 893% higher than that of the initial design. However, the improvement of P causes the remarkable reduction in the conversion efficiency η. Similarly, when taking η as the objective function, the increase in η for the optimal design also accompanies the significant reduction in P. Thus, the multi-objective optimization is necessary to improve P and η simultaneously. The present results confirm the effectiveness of the multi-objective optimization. With a weight factor of 0.5, the optimal design has $P = 0.39$ W and $\eta = 3.64\%$ at $I = 0.10$ A; $P = 1.04$ W and $\eta = 3.10\%$ at $I = 0.25$ A; $P = 1.27$ W and $\eta = 3.02\%$ at $I = 0.30$ A; $P = 1.16$ W and $\eta = 3.29\%$ at $I = 0.50$ A, which makes a reasonable balance between P and η to improve the both simultaneously.

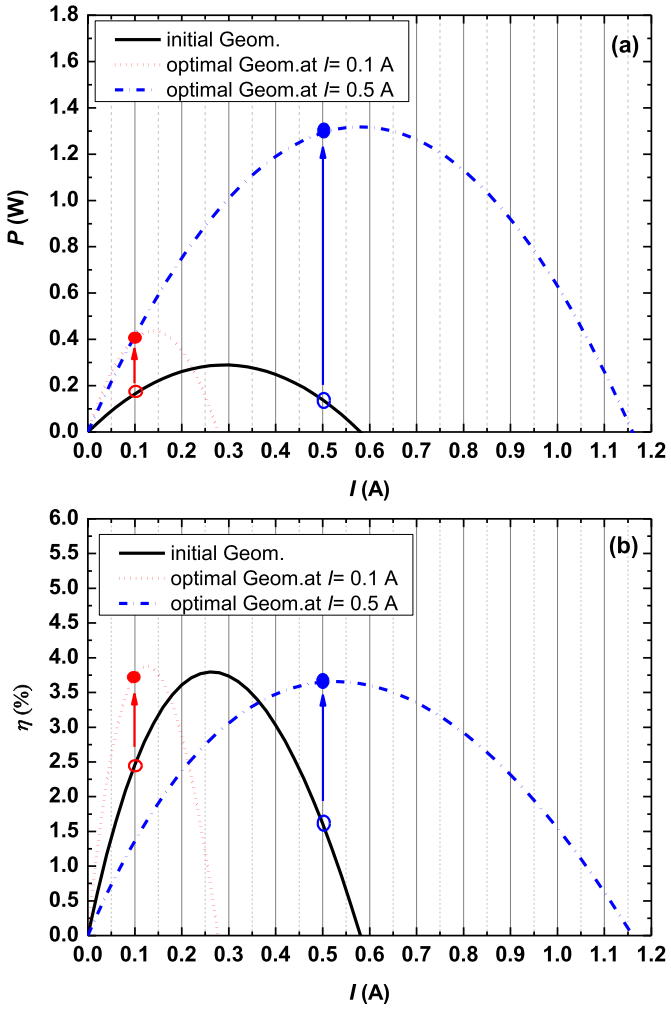

Fig. 11. Comparison of TEG performance between the initial and optimal designs: (a) P; (b) η.

Acknowledgment

This study was partially supported by the National Natural Science Foundation of China (No. 51276060), by the National Key Basic Research Program of China (No. 2012CB720401), and by the 111 Project (No. B13004).

References

[1] Disalvo FJ. Thermoelectric cooling and power generation. Science 1999;285:703–6.
[2] Chen WH, Wang CC, Hung CI, Yang CC, Juang RC. Modeling and simulation for the design of thermal-concentrated solar thermoelectric generator. Energy 2014;64:287–97.
[3] Sahin AZ, Yilbas BS. Thermodynamic irreversibility and performance characteristics of thermoelectric power generator. Energy 2014;55:899–904.
[4] Lua HL, Wu T, Bai SQ, Xu KC, Huang YJ, Gao WM, et al. Experiment on thermal uniformity and pressure drop of exhaust heat exchanger for automotive thermoelectric generator. Energy 2013;54:372–7.
[5] Bell LE. Cooling, heating, generating power, and recovering waste heat with thermoelectric systems. Science 2008;321:1457–61.
[6] Rowe DM, editor. Thermoelectrics handbook: macro to nano. Boca Raton: CRC Press; 2006.
[7] Riffat SB, Ma X. Thermoelectrics: a review of present and potential applications. Appl Therm Eng 2003;23:913–35.
[8] Minnich AJ, Dresselhaus MS, Ren ZF, Chen G. Bulk nanostructured thermoelectric materials current research and future prospects. Energy Environ Sci 2009;2:466–79.
[9] Tang XF, Zhang QJ. Synthesis and thermoelectric properties of p-type- and n-type-filled skutterudite $R_yM_xCo_{4-x}Sb_{12}$ (R: Ce, Ba, Y; M: Fe, Ni). J Appl Phys 2005;97:093712.
[10] Jang B, Han S, Kim JY. Optimal design for micro-thermoelectric generators using finite element analysis. Microelectron Eng 2011;88:775–8.
[11] Yu J, Zhao H, Xie K. Analysis of optimum configuration of two-stage thermoelectric modules. Cryogenics 2007;47:89–93.
[12] Chen J, Lin B, Wang H, Lin G. Optimal design of a multi-couple thermoelectric generator. Semicond Sci Technol 2000;15:184–8.
[13] Meng F, Chen L, Sun F. Performance optimization for two-stage thermoelectric refrigerator system driven by two-stage thermoelectric generator. Cryogenics 2009;49:57–65.
[14] Yilbas BS, Sahin AZ. Thermoelectric device and optimum external load parameter and slenderness ratio. Energy 2010;35:5380–4.
[15] Xuan XC, Ng KC, Yap C, Chua HT. Optimization of two-stage thermoelectric coolers with two design configurations. Energy Convers Manag 2002;43:2041–52.
[16] Cheng YH, Lin WK. Geometric optimization of thermoelectric coolers in a confined volume using genetic algorithms. Appl Therm Eng 2005;25:2983–97.
[17] Cheng YH, Shih C. Maximizing the cooling capacity and COP of two-stage thermoelectric coolers through genetic algorithm. Appl Therm Eng 2006;26:937–47.
[18] Rao RV, Patel V. Multi-objective optimization of two stage thermoelectric cooler using a modified teaching-learning-based optimization algorithm. Eng Appl Artif Intell 2013;26:430–45.
[19] Huan YX, Wang XD, Cheng CH, Lin DTW. Geometry optimization of thermoelectric coolers using simplified conjugate-gradient method. Energy 2013;59:689–97.
[20] Wang XD, Huang YX, Cheng CH, Lin DTW. A three-dimensional numerical modeling of thermoelectric device with consideration of coupling of temperature field and electric potential field. Energy 2012;47:488–97.
[21] Meng JH, Wang XD, Zhang XX. Transient modeling and dynamic characteristics of thermoelectric cooler. Appl Energy 2013;108:340–8.
[22] Meng JH, Zhang XX, Wang XD. Dynamic response characteristics of thermoelectric generator predicted by a three-dimensional heat-electricity coupled model. J Power Sources 2014;245:262–9.
[23] Meng JH, Zhang XX, Wang XD. Characteristics analysis and optimization of a thermoelectric generator by considering variable material properties and heat losses. Int J Heat Mass Transf; 2014. Submitted for publication.

[24] Cheng CH, Chang MH. A simplified conjugate-gradient method for shape identification based on thermal data. Numer Heat Transf 2003;43:489–507.
[25] Wang XD, Huang YX, Cheng CH, Jang JY, Lee DJ, Yan WM, et al. An inverse geometry design problem for optimization of single serpentine flow field of PEM fuel cell. Int J Hydrogen Energy 2010;35:4247–57.
[26] Wang XD, An B, Xu JL. Optimal geometric structure for nanofluid-cooled microchannel heat sink under various constraint conditions. Energy Convers Manag 2013;65:528–38.
[27] Martinez A, Astrain D, Rodriguez A. Dynamic model for simulation of thermoelectric self-cooling applications. Energy 2013;55:1114–26.